Chapter 3

Ka-to-W Band EM Wave Propagation: Tropospheric Effects and Countermeasures

Lorenzo Luini, Roberto Nebuloni and Carlo Riva

Additional information is available at the end of the chapter

http://dx.doi.org/10.5772/66660

Abstract

Near future satellite and terrestrial telecommunication (TLC) systems are expected to benefit from the use of operational frequencies spanning the Ka, Q, V and W bands, the main advantages being the availability of larger bandwidths and the smaller antenna size for a given gain. Moreover, the possibility of using on-board antennas with enhanced directivity is attractive for satellite systems whose coverage area is subdivided into spot beams for frequency reallocation or regional services. For example, the W band is attractive for fixed satellite services (FSS), especially for geostationary high-throughput systems (HTSs), in which the use of such frequencies for the feeder link (i.e. large available bandwidth) could reduce significantly the number of gateways with respect to Ka and Q/V bands. As for deep space missions, the main driver for the interest in using frequencies in the Ka to W bands is the possible increase in the on-board antenna gain with respect to the values at X band considered for current or planned missions. The drawback of using electromagnetic waves at frequencies in Ka, Q, V and W bands is the definite impact of the impairments caused by the troposphere. As a consequence, the design of TLC systems at such frequencies, and in particular satellite-based ones, cannot rely on the classical approach of simply assigning an extra power margin to counteract atmospheric fades. The extensive use of fade mitigation techniques (FMTs), such as link power control (LPC), site diversity or on-board adaptive power allocation, from the propagation side, adaptive coding and modulation (ACM) and data rate adaptation (DRA), from the telecommunication side, is mandatory. A reduction of the quality of service (QoS) should also be considered. This chapter deals with all these aspects characterizing the propagation of electromagnetic waves in the Ka, Q, V and W bands, spanning from the main impairments induced by the troposphere (and how they change as the frequency increases), to how extreme atmospheric conditions can be handled making use of suitable FMTs.

Keywords: electromagnetic wave propagation, atmospheric effects, satellite communications, fade mitigation techniques

1. Tropospheric effects at Ka band and above

Satellite and terrestrial telecommunication (TLC) using very high frequency bands (Ka band and above) benefit from the available larger bandwidths and the smaller antenna size for a fixed gain or the larger gain for a fixed antenna size. Unfortunately, radiowaves at Ka band and above are more severely affected by impairments due to tropospheric elements [1–4] and, in particular, gases, clouds, rain and turbulence.

Oxygen and water vapour are the relevant gaseous components for radio wave propagation in the 20–300 GHz frequency range. Oxygen attenuation is weakly dependent on temperature and atmospheric pressure and its space and time variations are quite limited. The dependence on frequency is much larger with a resonant absorption band at 60 GHz (with specific attenuation that can exceed 10 dB/km) and smaller absorption (less than 0.1 dB/km) below 40–50 GHz and above 70–80 GHz. The water vapour absorption strongly depends on temperature, pressure and humidity, exhibiting marked daily, seasonal and geographical variations. Water vapour-specific attenuation is characterized by a broadened peak around the H_2O absorption line at 22.2 GHz (up to about 0.2 dB/km in reference conditions[1]) and monotonically increases in the 40–100 GHz band (up to about 1 dB/km in reference conditions). As shown in **Figure 1** [5], the specific gas (oxygen and water vapour) attenuation in reference conditions is around 0.1 dB/km (with a peak of 0.2 dB/km at 22.2 GHz) in Ka band, while it increases with frequency from 0.1 to 0.4 dB/km in Q/V band. Due to the opposite

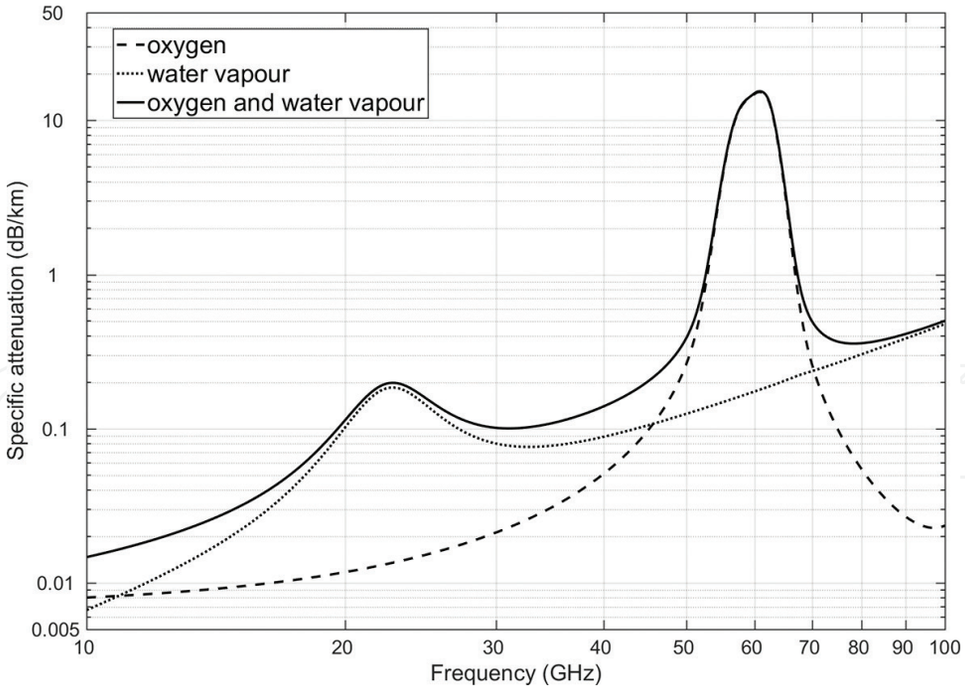

Figure 1. Oxygen (dashed line), water vapour (dotted line) and total gas (solid line) specific attenuation at reference conditions (water vapour density 7.5 g/m3, temperature 15°C, atmospheric pressure 1013 hPa).

[1]Temperature 15°C, pressure 1013 hPa, water vapour density 7.5 g/m3 [5].

http://dx.doi.org/10.5772/66660

dependence of oxygen and water vapour attenuation on frequency, the specific gas attenuation in the W band is included in the interval between 0.36 and 0.5 dB/km, being higher at the bandwidth edges (70 and 95 GHz) and lower in the centre. The total gas attenuation along a slant path depends on the atmospheric profile of temperature, relative humidity and pressure. The models currently recommended by the International Telecommunication Union-Radiocommunication (ITU-R) sector for the prediction of the slant path gas attenuation [5] rely on solid physical bases and are expected to be quite accurate at least up to 100 GHz. Such models introduce simplifications relying on the description of vertical profiles of oxygen and water vapour concentrations by using effective parameters, like the oxygen effective height (analytical function of frequency and pressure) and the water vapour total content (global maps of this parameter are available in Ref. [6]). The mean yearly distribution of oxygen and water vapour attenuation at the zenith is calculated by multiplying their specific attenuation (in reference conditions) by the effective parameters and the slant path attenuation is then obtained through the cosecant law, reasonably assuming the local homogeneity of the atmosphere. As an example, the predicted zenith gas attenuation exceeding 1% of the average yearly time at 20 (Ka band), 50 (V band) and 80 (W band) GHz ranges almost all over the globe in the intervals 0.1–1, 1-2.5 and 1–3 dB, respectively.

In non-precipitating atmosphere, the attenuation due to clouds must be also considered. Since in the 10–100 GHz band the size of suspended water droplets in clouds is smaller than the wavelength, the extinction cross sections can be calculated by using the Rayleigh approximation, according to which the cloud attenuation turns out to depend only on the liquid water content, on the droplets temperature and on frequency. Cloud attenuation changes with climate and reveals a large temporal variability, depending on the presence of clouds along the link and on their liquid water content. It is monotonically increasing with frequency in the 10–100 GHz band. In ITU-R recommendation P.840-6 [7], cloud attenuation is calculated through the reduced liquid water total content (kg/m^2) or (mm), an effective parameter that depends on frequency and is available through global maps (presently calculated for the 20–50 GHz band) [7]. Cloud attenuation depends also on the water permittivity, the frequency and the elevation angle. The predicted zenith cloud attenuation exceeding 1% of the average yearly time at 20 GHz does not exceed 2 dB all over the globe, while it can exceed 10 dB in equatorial and tropical regions at 80 GHz, as shown in **Figure 2**. It is then clear that, even in absence of rain, cloud attenuation only limits availability in the W band.

As for precipitating atmosphere, the wavelength above 10 GHz becomes comparable to the size of hydrometeors (few millimetres), causing absorption and scattering, and consequently attenuation, of the incident wave. The rain attenuation along a slant path can be calculated by integrating the specific attenuation, which statistically depends on rain intensity, R (mm/h), as follows:

$$\gamma = kR^{\alpha} \tag{1}$$

In Eq. (1), k and α are coefficients (provided, for instance, in recommendation ITU-R P.838-3 [8]), which depend on frequency, elevation angle, drop temperature, wave polarization (as raindrops are not spherical), drop size distribution (DSD) and shape. DSD and shape can vary during a single event or from one event to the other, leading to significant differences in specific rain attenuation. In the W band, the effect of the DSD is more evident than in the

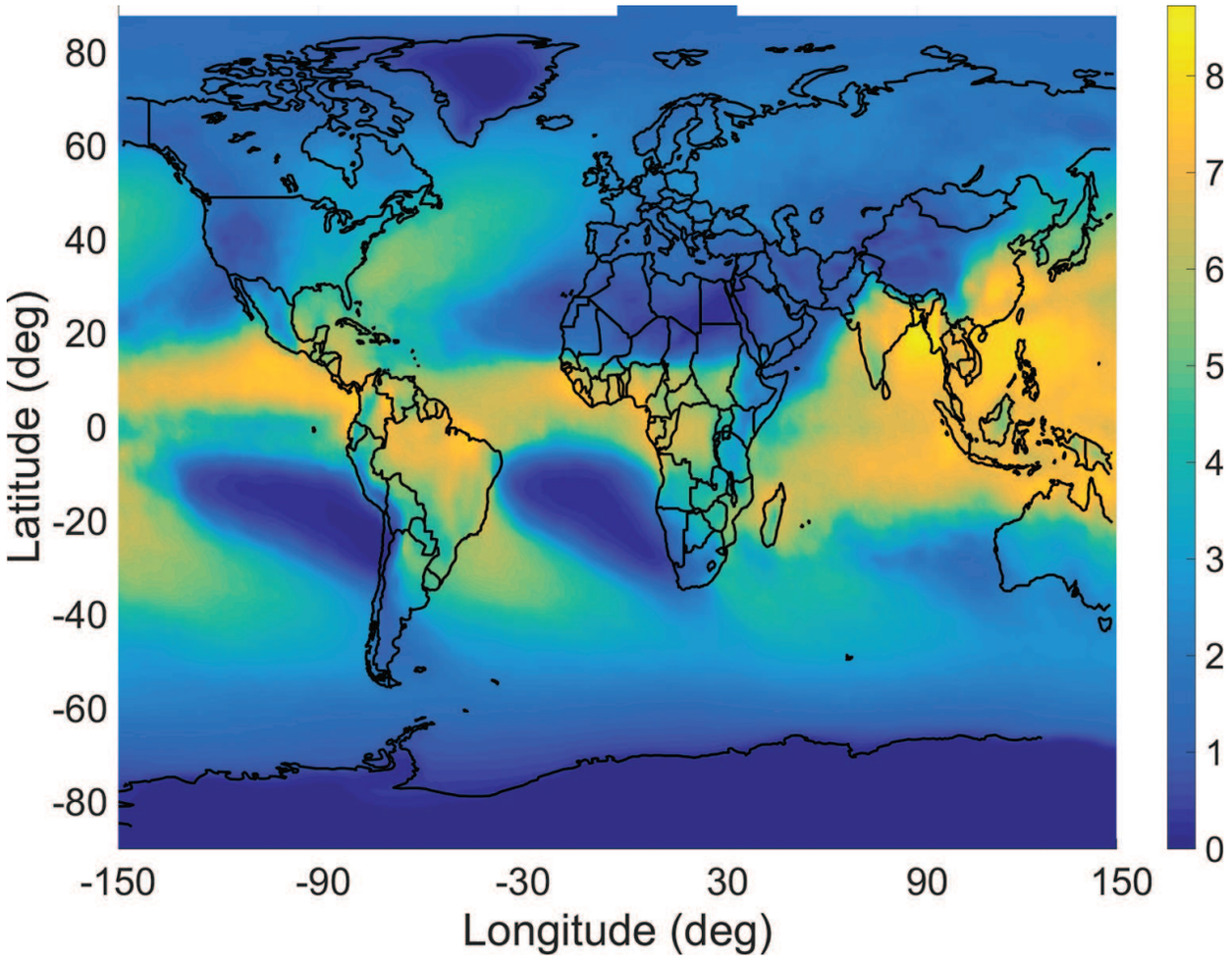

Figure 2. Zenith cloud attenuation (dB) at 80 GHz exceeded for 1%, prediction according to recommendation ITU-R P.840-6 [7].

lower bands, with a marked dependence on rain intensity: for example, at 10 mm/h, the peak to peak relative variation of the specific attenuation for various DSD is about 40% (for both polarizations). The difference between specific attenuation in vertical and horizontal polarization is well below 5%. As for the prediction of rain attenuation in the 10–100 GHz band, the k and α coefficients in Ref. [8] can be used, though they originate from a best-fitting procedure up to V band, and their accuracy in W band is still to be verified.

The rain attenuation exceeded for a certain time percentage in a year is related to the local rain rate exceeded for the same percentage, which may vary significantly across the globe; as an example, **Figure 3** shows the global map [9] of the rain rate (mm/h) exceeded for 0.01% of the average year (which corresponds approximately to 1 h in a year). The probability to have rain, P_0, is very close to the probability to have rain attenuation, P_A; typically, for temperate climate, $P_0 \approx 4$–8% [9], and $P_A \approx 6$–10%, depending on the link elevation angle.

Several models have been developed in the last decades to predict rain attenuation statistics from the local rain rate statistics. Their accuracy in the 10–50 GHz range [10] is generally satisfactory. Since experimental statistics from earth-to-satellite links are not available for prediction models testing above 50 GHz, in this frequency range, physically based methods should

http://dx.doi.org/10.5772/66660

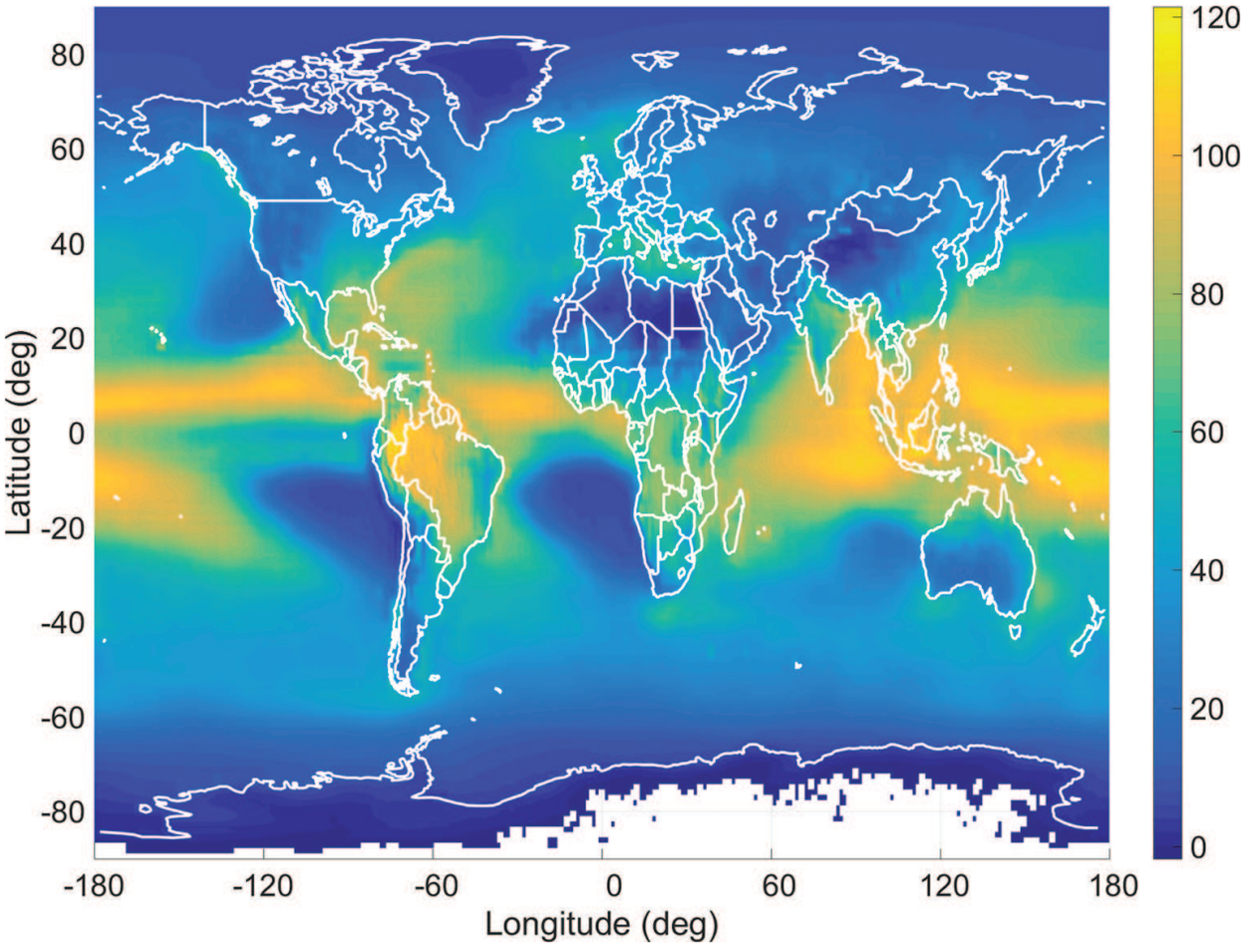

Figure 3. Global map of rain rate (mm/h) exceeded for 0.01% of the average year.

be privileged, as their accuracy is not expected to depend significantly on the frequency. The SC EXCELL (Stratiform Convective EXponential CELL) model [11, 12], for example, describes the precipitation through a set of synthetic isolated rain cells with exponential rain rate profile; moreover, SC EXCELL takes separately into account stratiform and convective rain contributions, using different rain heights for the two types of precipitation. Finally, the contribution due to melting layer (the layer, lying just on the top of rain, where snow and ice particles gradually melt during their fall to the ground) is added only to stratiform rain through an equivalent rain slab whose height depends on frequency. **Figure 4** shows an example of rain attenuation statistics (specifically, the complementary cumulative distribution function [CCDF]) predicted by SC EXCELL for a satellite slant path (elevation angle 35°) at 20, 50 and 80 GHz (vertical polarization). It is evident from the figure that, due to rain effects only, a system availability of 99.99% (outage of 0.01%) is realistic only in Ka band (20 GHz), with a propagation power margin of about 20 dB. In V (50 GHz) and W (80 GHz) band, a maximum availability of 99% is probably feasible, if no adequate fade mitigation techniques (FMTs) are implemented.

In case of dual polarization systems, another effect induced by rain must be taken into account: depolarization (specifically, cross polarization discrimination, XPD), which is introduced by non-spherical drops. It is worthwhile observing that anisotropic ice crystals also produce the

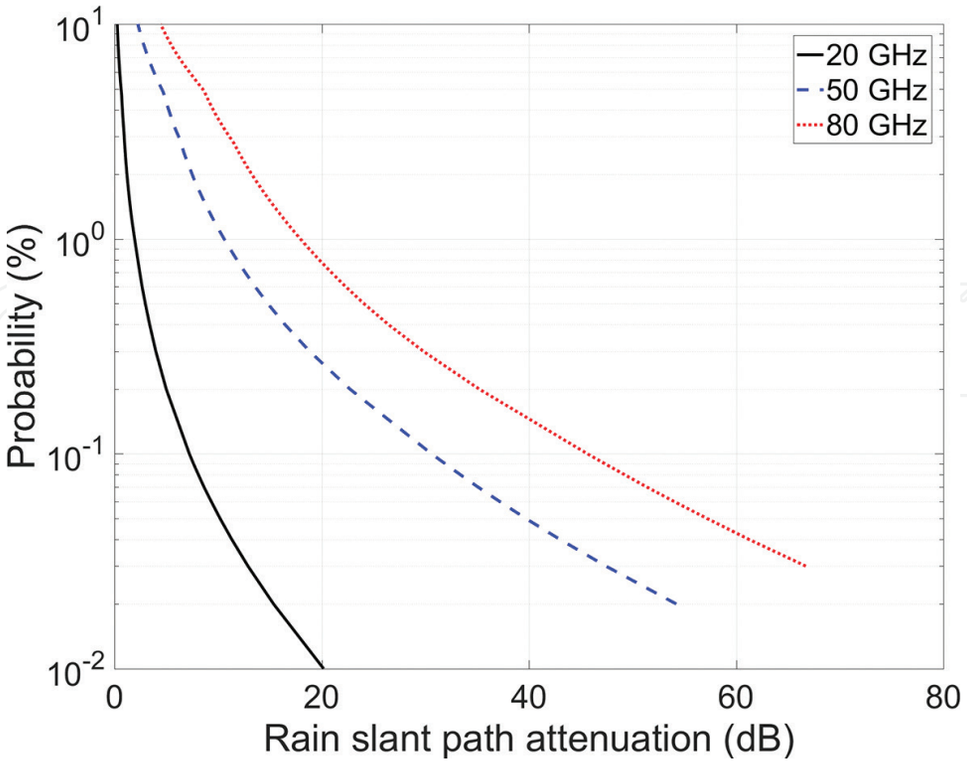

Figure 4. CCDF of rain attenuation (predicted by the SC EXCELL model [11]) for a satellite slant path (elevation angle 35°) from a ground station located in Milano (lat. 45.5°N, long. 9.2°E, alt. 120 m a.m.s.l.) at 20 GHz (black solid line), 50 GHz (blue dashed line) and 80 GHz (red dotted line) with vertical polarization.

same effect in presence or absence of rain. The physical parameters that cause XPD are the anisotropy (i.e. the polarization dependent forward scattering of the particles, both for hydrometeors and ice crystals) and the angle of the symmetry axes of the particles with respect to the polarization plane, named canting angle. Like rain attenuation, also XPD increases dramatically with the frequency; by scaling anisotropies, it is possible to scale depolarization with frequency [13]. The hydrometeor axes, however, are not equi-aligned, and the dispersion of these orientations generally reduces the XPD. This aspect and the co-presence of water and ice particles along the path makes the depolarization phenomenon complex and difficult to describe. Ice XPD is the critical issue for low margin systems at high frequencies (above Ka band) since, during rainy periods, the system is probably already in outage. On the other hand, the XPD due to rain can have an impact when attenuation is close to the fade margin of gateway systems with high availabilities.

Finally, turbulence effect must be mentioned. Turbulent eddies in the troposphere cause small-scale inhomogeneity of the atmospheric refractive index along the propagation path, which produces signal scintillation, that is, rapid fluctuations of the received signal amplitude, above about 10 GHz. Scintillation, when expressed in decibels, is characterized by a Gaussian distribution with a stationary standard deviation over few minutes. In turn, scintillation standard deviation depends on the turbulence structure index; it increases with the frequency (but much less than rain attenuation) [14] and with the path length, and it decreases with the increasing antenna size, due to the aperture averaging effect. Scintillation can also

http://dx.doi.org/10.5772/66660

be due to the variation of the arrival angle of the main ray; in this case, it increases with the decreasing beamwidth as a result of the effect of the antenna radiation pattern [14]. The impact of scintillation, typically quite smaller than that of attenuation, can be important for low elevation angles and low margin systems. Moreover, scintillation can interfere with tracking systems or fade mitigation techniques. Scintillation can also occur during rain events and, in this case, the signal variations are mixed with the fast fluctuations induced by rain itself.

2. Fade mitigation in the Q/V feeder link channel

The actual generation of fixed satellite services (FSS) for TLC applications (e.g. Eutelsat KA-SAT and Hughes EchoStar XVII) achieve throughputs of the order of 100 Gbit/s by exploiting full Ka-band operation, multibeam architectures with frequency reuse on the user link side, and a number of high-capacity gateway (GW) links on the feeder link side. A further increase in the capacity of future HTS by an order of magnitude up to the Terabit/s is now under investigation as it would be supported by the growing market demand for broadband access [15]. However, it involves several technological challenges as well. Designing the general architecture of an HTS is a complex task and it is beyond the scope of this chapter. Here the focus is on the impact of the propagation channel on the design of the feeder link, that is, the connection between the GW station and the satellite. To this aim, a reference scenario for a future HTS is sketched and the most suitable FMTs to counteract atmospheric attenuation are reviewed.

2.1. Number of beams

A simple calculation of the required number of GW beams and user beams to achieve Terabit/s capacity can be carried out once the available bandwidth, the frequency reuse scheme and the modulation scheme are given. An important assumption is that the traffic is uniform, that is, the system capacity is shared in equal parts among the user beams as well as among the GW beams. If the same MODCOD (MODulation and CODing) is transmitted, the relationship between total satellite capacity C_{tot} (one-way) and number of user beams N_{UB} is given as:

$$C_{tot} = N_{UB} \frac{N_p}{F} B \times SE \tag{2}$$

where N_p is the number of polarizations, F is the frequency reuse factor, B is the bandwidth per beam, and SE is the spectral efficiency of the MODCOD. For instance, assuming B = 0.5 GHz/beam, that is, the entire exclusive bandwidth available for FSS across the European Community [16], SE = 3.433 (corresponding to the 32 APSK 5/6), N_p = 2 and F = 4, we obtain

$$N_{UB} = C_{tot} \frac{F}{N_p} \frac{1}{B \times SE} = 500 \frac{4}{2} \frac{1}{0.5 \times 3.433} = 583 \tag{3}$$

being the 1 Terabit/s shared between uplink and downlink. Furthermore, the capacity on the user link side must equal the one of the feeder link, that is

$$C_{GW} N_{GW} = C_{UB} N_{UB} \tag{4}$$

In the Q-V band, a much larger bandwidth (4–5 GHz) would be available even though in Europe there are no exclusive bandwidths for FSS [16]. Assuming that each GW has the entire Q-V bandwidth at its disposal, that is, $B = 4$ GHz, and $SE = 3.433$, $N_p = 1$ and $F = 1$, the required number of GW beams would approximately be equal to

$$N_{GW} = 500 \frac{1}{4 \times 3.433} = 36 \tag{5}$$

Hence, each GW would serve 4×2/0.5 = 16 user beams.

In the design practice, other factors contribute to find the optimum number of spots, such as available on-board power, complexity of the on-board antenna system, interference issues, etc.

2.2. Space diversity

The drawback of higher frequencies, specifically Q/V-band, is the increased vulnerability to the propagation impairments. Rain fades at Q/V-band are much larger than the dynamic range of receiver systems with typical feeder link availability targets (99.9%), even when uplink power control is featured. To this aim, a well-known FMT is single site diversity (SSD), where a GW is backed up by an idle GW located within the same feeder beam (**Figure 5**).

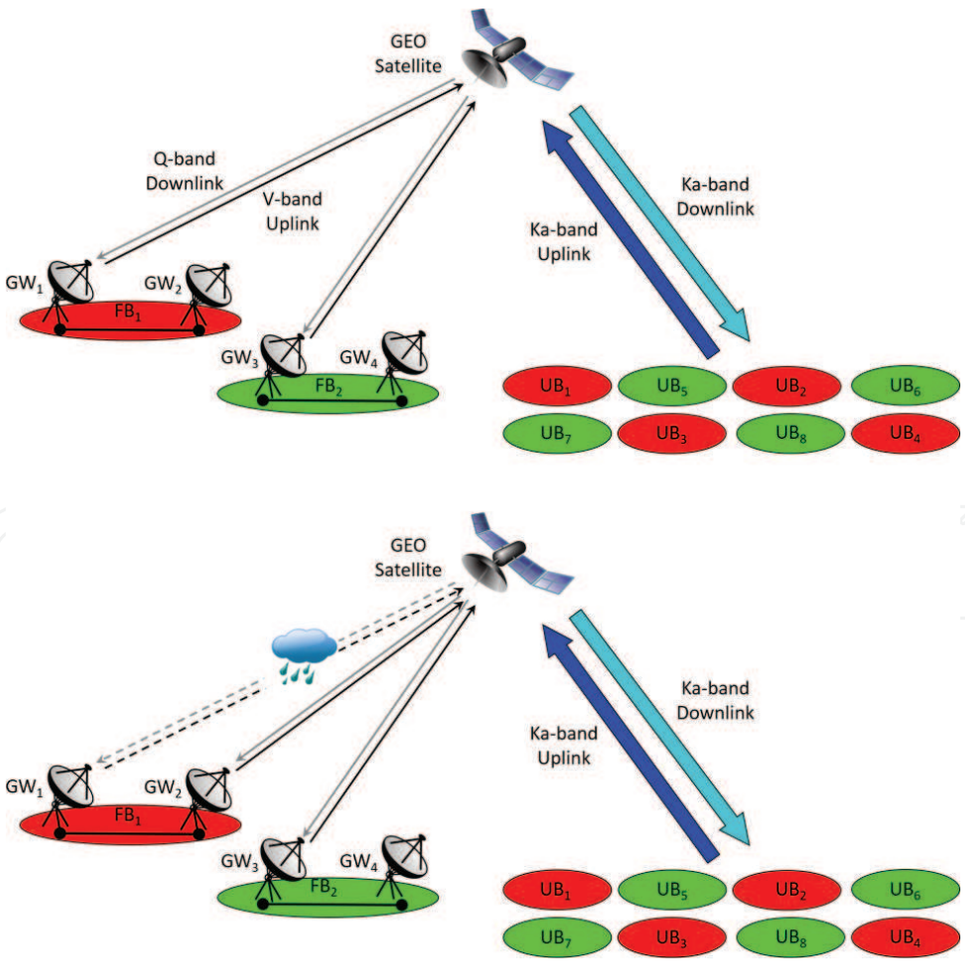

Figure 5. Single site diversity across the feeder link of an FSS.

http://dx.doi.org/10.5772/66660

When GW_1 is faded, the traffic is switched to GW_2 which transmits the same set of carriers as GW_1. The payload is therefore transparent to the process of allocating users from the GW in outage to the idle GW (switchover). The higher the distance between GW_1 and GW_2 the lower the probability that both are faded.

Conventional SSD, relying on the availability of an idle GW to back up a faded GW, is not a cost-effective solution when many GWs are required to convey the user beams traffic, as it basically doubles the cost of the ground segment. On the other side, the diversity scheme in **Figure 6** achieves the required availability target while minimizing the number of redundant GWs with respect to SSD. There are N operational GWs and $P < N$ redundant GWs ($N = 2$ and $P = 1$ in the figure, for the purpose of illustration), each located within its own feeder beam. The redundant capacity provided by the P back-up GWs is shared among the user beams: when one of the operational GWs (GW_1 or GW_2) is faded, it is replaced by GW_3. The above "$N + P$" scheme tolerates up to P GWs in outage with no loss of capacity. As a drawback, $N + P$ implies a higher degree of complexity both on the ground segment and on-board. In fact, the GWs must be interconnected by high-speed fibre optic links to form a smart-gateway network (SGN). For instance, in **Figure 6**, the GWs nodes form a star topology where the central node, namely the

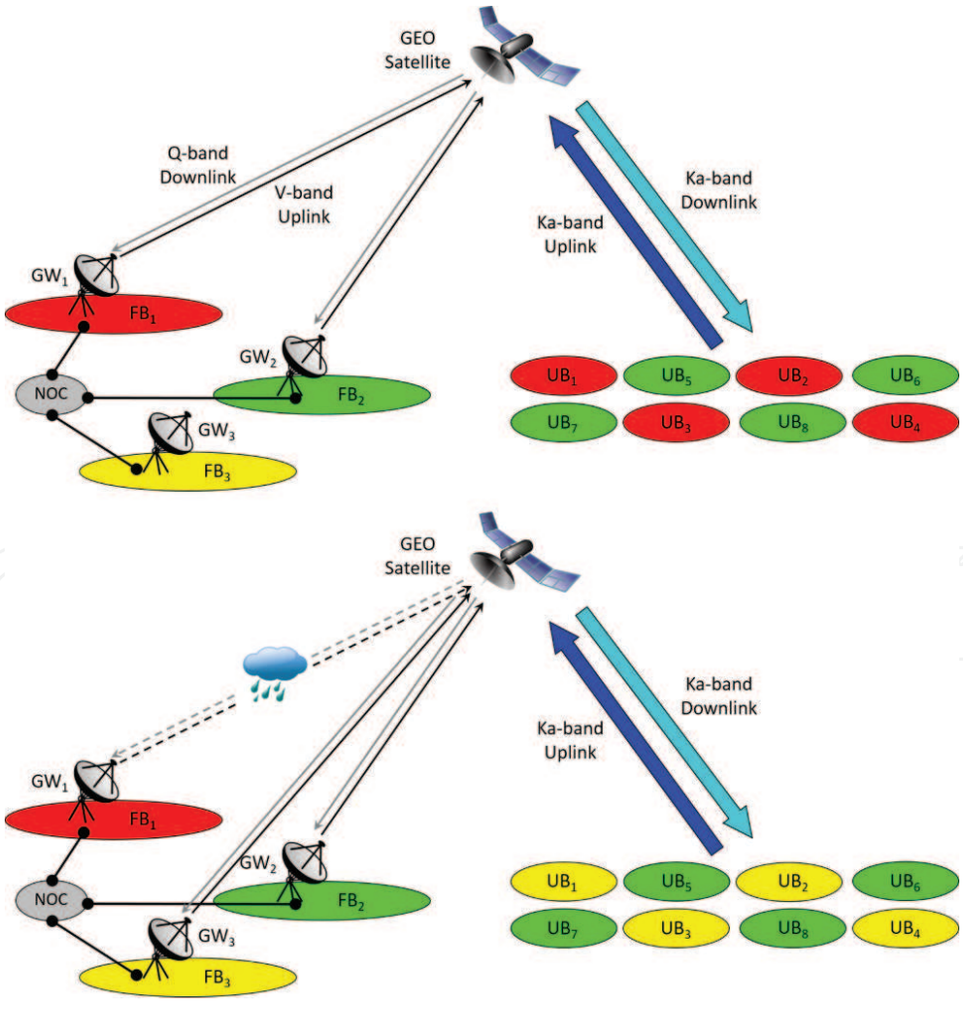

Figure 6. $N + P$ diversity scheme across the feeder link of an FSS.

network operation centre (NOC), carries out resource management and controls traffic switchover. Moreover, the payload should host $N + P$ (instead of N) receiver-transmitter front-end chains and should provide rerouting capability from every user beam to any of the back-up GWs. In general, a trade-off between flexibility in managing system resources and complexity (both ground segment and payload) must be addressed.

With SSD and N + P diversity, a user beam is served by a single GW at a time. More complex diversity schemes have been proposed as well, where a single user-beam is connected to several GWs at a time through frequency division multiple access (FDMA) [17]. When a GW is in outage, the user beam traffic conveyed by its carriers is switched to a different GW serving the same set of beams as the faded GW. If the system does have some redundancy (i.e. unused carriers in ideal conditions), an outage event does not imply a loss of capacity. These solutions are more challenging than $N + P$ as they envisage a number of complex tasks including evaluation and distribution of the available resources, signalling and synchronization to the new carrier and assignment of the user terminals among the new set of carriers.

2.3. $N + P$ performance

Let us now assess the effectiveness of $N + P$ in mitigating the impact of the atmospheric channel on the Q-V band feeder link for the reference scenario described above. The following figures of merit are considered:

- The propagation margin, that is, the extra decibel margin to be included in the link budget equation to guarantee a targeted feeder link availability.
- The duration and the rate of fades, which, in turn, have an impact on the algorithms controlling the switchover process.

The propagation margin can be calculated from the CCDF of rain attenuation at each GW site and basic statistical theory, provided that the rain process is assumed to occur independently over different GW links. On the other side, a full characterization of the propagation channel can be carried out only by models able to generate realistic time series of attenuation in every GW site, possibly taking into account the correlation of the rain process in time and space. Here, we have used the multisite time series synthesizer (MTS) proposed in Ref. [18] to simulate the rainy atmospheric channel for a V-band (50 GHz) feeder link (we consider here uplink only). The MTS generates synthetic time series of rain attenuation across an arbitrary ensemble of slant paths up to the V-band by combining series of measured data carried out during the ITALSAT propagation campaign. First-order statistics are reproduced and the spatial correlation of rain is duly taken into account. The contribution of non-rainy components, that is, clear-sky attenuation, is obviously non-negligible at V-band, as shown in the first part of this chapter. However, clear-sky attenuation is on the order of few decibels and though time variant, its fluctuations can be managed by FMTs such as uplink power control. On the other side, the peaked and fast fades produced by rain prompt for an approach based on space diversity.

Without loss of generality, let us consider a system of 10 GWs operating in a 9 + 1 diversity scheme. In fact, the 36-GW system necessary to achieve the Terabit/s capacity could be divided into four independent clusters of 9 + 1 GWs each. Indeed, this architecture would

http://dx.doi.org/10.5772/66660

result in a decrease in the number of high-speed connections among the GWs, with respect to, for example, a 36 + 4 diversity scheme. The 10 selected GW sites are reported in **Table 1**, assuming a GEO satellite providing continental coverage across Europe, alongside the climatologic probability of rain and the slant-path rain attenuation exceeded for 0.1 and 0.01% of time, respectively. The distance between the stations that should be maximized in the design process ranges from less than 500 km to about 3200 km.

Id	Site	Lat. (°)	Lon. (°)	Alt. (m)	P_0 (%)	0.1%	0.01%
1	Helsinki	60.1697	24.9383	5	3.55	19.1	49.8
2	Berlin	52.5192	13.4058	48	3.43	17.0	45.7
3	Cork	51.8967	−8.4861	20	7.85	22.3	51.9
4	Trieste	45.6494	13.7778	28	6.51	28.9	68.0
5	Athens	37.9836	23.7292	75	3.85	17.5	46.6
6	Cyprus	35.1264	33.4297	122	1.47	24.7	68.5
7	Turin	45.0628	7.6783	235	5.98	25.5	61.6
8	Paris	48.8564	2.3522	48	4.68	18.0	45.6
9	Madrid	40.4167	−3.7036	655	2.98	13.1	37.1
10	Cagliari	39.2236	9.1217	46	1.94	14.7	45.8

GEO satellite located at 9°E.

Table 1. Coordinates, altitude, probability of rain and 50-GHz slant-path rain attenuation (in dB) in 10 sites throughout Europe.

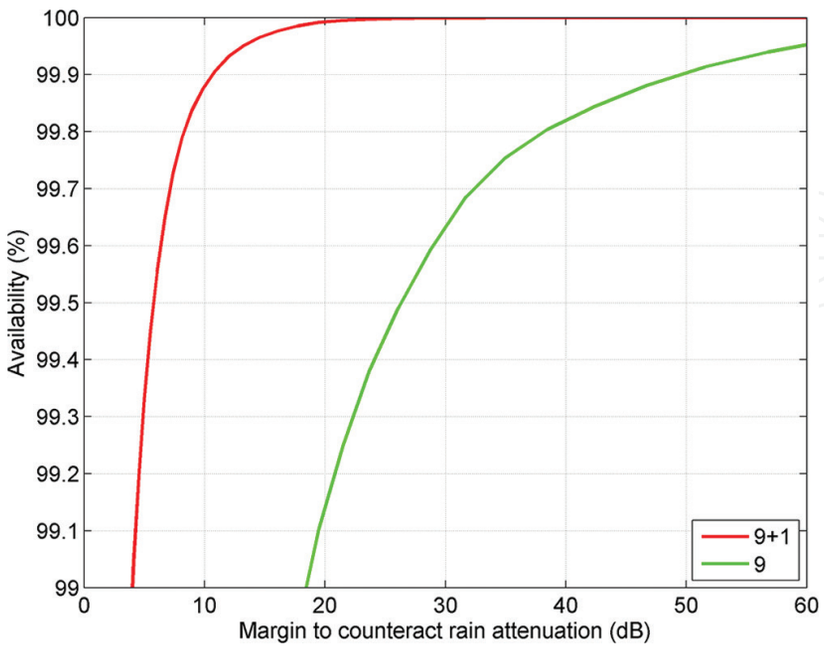

Figure 7. Performance of the 9 + 1 diversity scheme at V-band.

Figure 7 shows the benefits of 9 + 1 diversity with respect to a 9 + 0 system, used here only as a benchmark, in terms of the reduction of the required margin against rain fades that must be included in the link budget. For a typical feeder link availability of 99.9%, a 9 + 1 system requires a 10.7 dB margin against an unfeasible 50 dB, if the 9 + 0 system was operational for 99.9% of time. The 9 + 1 curve has been obtained as follows: (a) generate the time series of rain attenuation taking (in every sampling time) the second-worst value of attenuation among the ten GW links and (b) build the CCDF of the resulting time series. The underlying assumption is that instantaneous switchover is feasible.

The characteristics of fades are crucial for implementing the algorithms that control traffic switchover from a GW in outage to another. The operation involves higher layer network operations; hence, it is a good practice to design the diversity scheme in order to minimize the switching rate. Moreover, switching algorithms must be robust to short and intense signal fades that are more likely to occur at such high frequencies. Thresholding methods based on hysteresis are a simple solution that prevents from switching triggered by false alarms. The switchover will be carried out when signal attenuation across an operational link exceeds a certain value, namely a certain fade depth *D*. The statistics of events exceeding *D* can be calculated in several different ways. Here the distribution of the number of fades longer than *D* is calculated over an average year as generated by the MTS.

If we target a 99.9% availability, from **Figure 7**, the system margin against rain fades is 10.7 dB at V-band, which means that a fade depth equal to (or greater than) 10.7 dB occurring at the same time across two links produces system outage. **Figure 8** shows the distribution of fade durations corresponding to a fade depth equal to 10.7 dB. A fade occurring across a

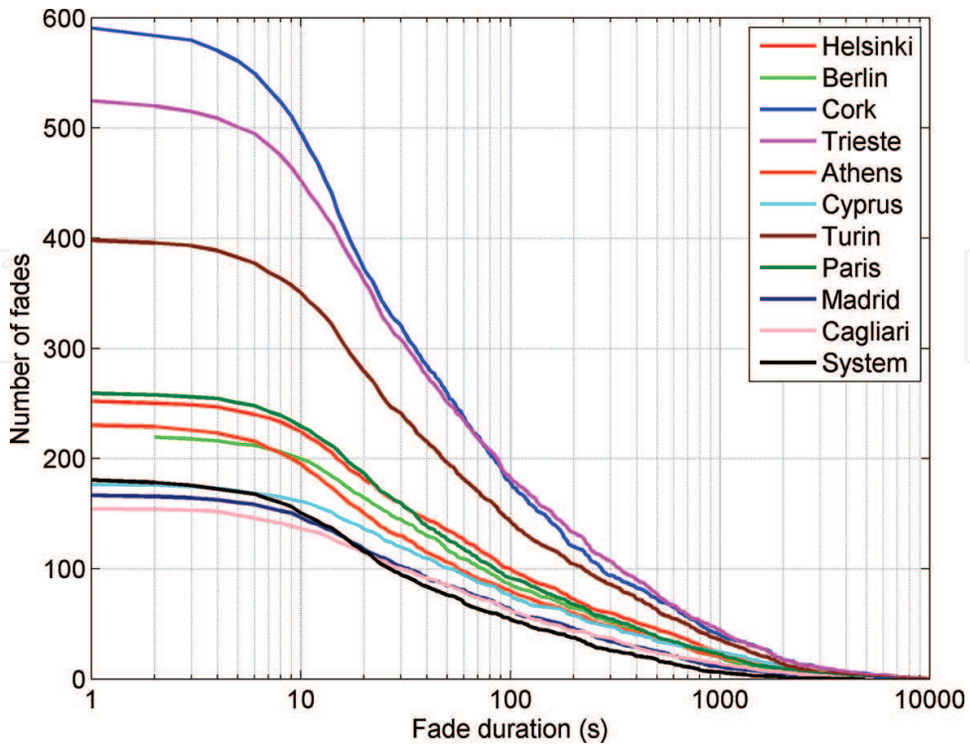

Figure 8. Number of fades exceeding a 10.7 dB depth (corresponding to 99.9% availability) in a 9 + 1 diversity scheme at V-band.

http://dx.doi.org/10.5772/66660

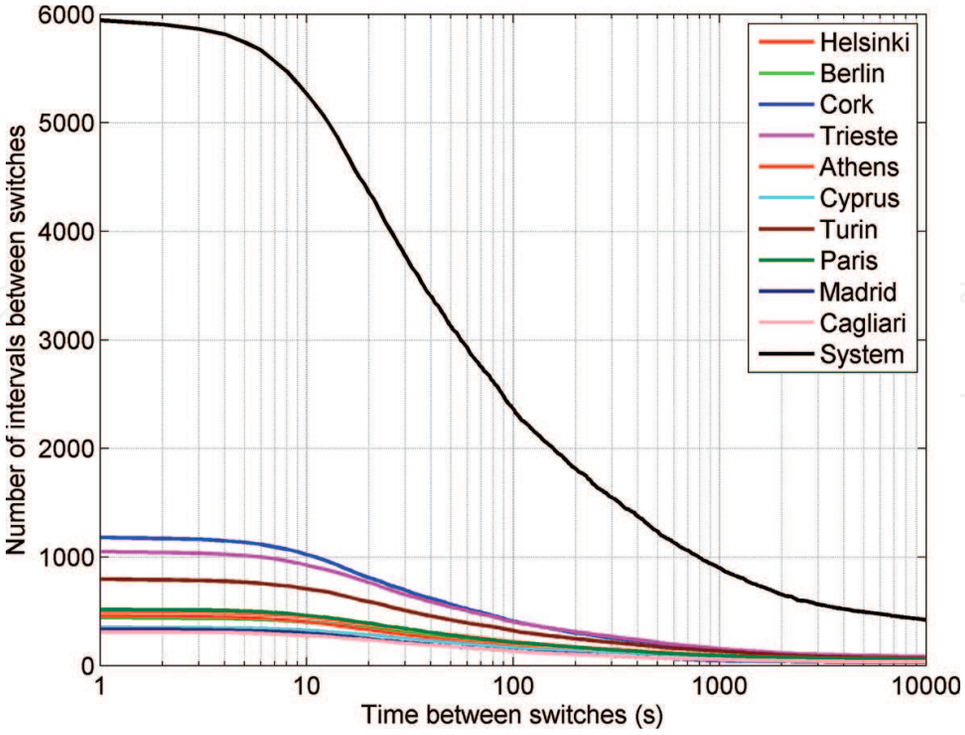

Figure 9. Number of intervals between switchovers in a 9 + 1 diversity scheme at V-band. Availability: 99.9%.

certain link is counted only if it does not produce system outage. The curves of the individual links are similar to the ones obtained as if they were operating independently of each other (not shown here). If the curves were normalized to the total number of fades, they would be packed together. Indeed, it is known that the relative occurrence of fades of different duration is rather site independent, whereas the number of fades of a given duration obviously is not.

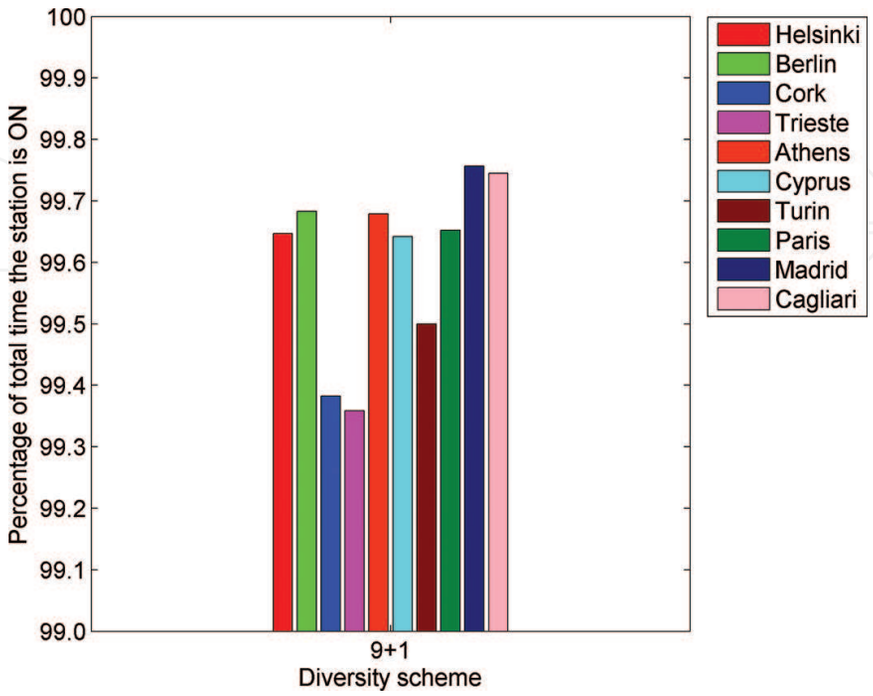

Figure 10. In-service time of each GW in a 9 + 1 diversity scheme at V-band. System availability: 99.9%.

Finally, the curve labelled "system" refers to the fades detected in the time series of attenuation built-up considering the best nine links (assuming instantaneous switching).

Figure 9 shows the distribution of the time intervals between consecutive switches for each GW in the 9 + 1 diversity scheme. In the average year, the system is expected to operate about 6000 switchovers, that is, approximately, once every 1.5 h. However, a non-negligible percentage of switchovers must be carried out in few seconds.

Finally, **Figure 10** shows the ratio of the time during which each link is operational normalized to the time when the system is operational. Note that operation time (hence the resources) is rather uniformly shared among the stations. Lower operation times correspond to the stations that exhibit worse CCDFs of rain attenuation.

3. Fade mitigation in the Ka band user link channel

As discussed above, the $N + P$ diversity scheme is much more cost-effective than SSD, which, on the contrary, represents a viable solution to significantly improve the system performance on the user link side (typically operating in the Ka band [16]), especially when such a user requires a reliable broadband service (e.g. emergency applications). Indeed, a two-site diversity system for the user link with stations at a distance ranging between 20 and 50 km typically allows a considerable increase in the link availability (reduced outage time) and/or performance (increased data rates) [19], mainly associated to the strongly uneven spatial distribution of precipitation.

In order to properly estimate the advantage achievable with such a kind of system, reliable and accurate propagation models are required, especially when limited propagation data are available to test their accuracy. To this aim, a combination of physically based models can be used: MultiEXCELL (Multi EXponential CELL) to synthesize rain rate fields [20], SMOC (Stochastic MOdel of Clouds) to reproduce cloud fields [21] and SMOV (Stochastic MOdel of water Vapour) to generate water vapour fields [22]. As preliminary shown in Ref. [23], these diversified synthetic fields can be combined (including the constant attenuation due to oxygen, whose variability in time and space is extremely low) so as to maintain the local first-order (i.e. CCDF) and second-order (i.e. spatial correlation) statistics of the single atmospheric elements, as well as to preserve their mutual correlation (e.g. clouds covering areas affected by precipitation and higher water vapour content where clouds lie). This is exemplified in **Figure 11**, which depicts a sample cloud field (vertical integrated liquid water content) and the associated water vapour field (vertical integrated water vapour content), as well as in **Figure 12**, which shows that the synthetic fields generated by MultiEXCELL, SMOC and SMOV also take into account the vertical development of rain rate, clouds and water vapour to allow a more realistic simulation of the interaction between electromagnetic waves and the atmosphere. This not only means a direct combination of the impairments due to the various constituents in the atmosphere (in contrast to the statistical approach proposed in recommendation ITU-R P.618-12 [24] to combine the attenuation due to clouds, rain and gases), which is expected to increase the prediction accuracy, but also provides a high flexibility of the model,

http://dx.doi.org/10.5772/66660

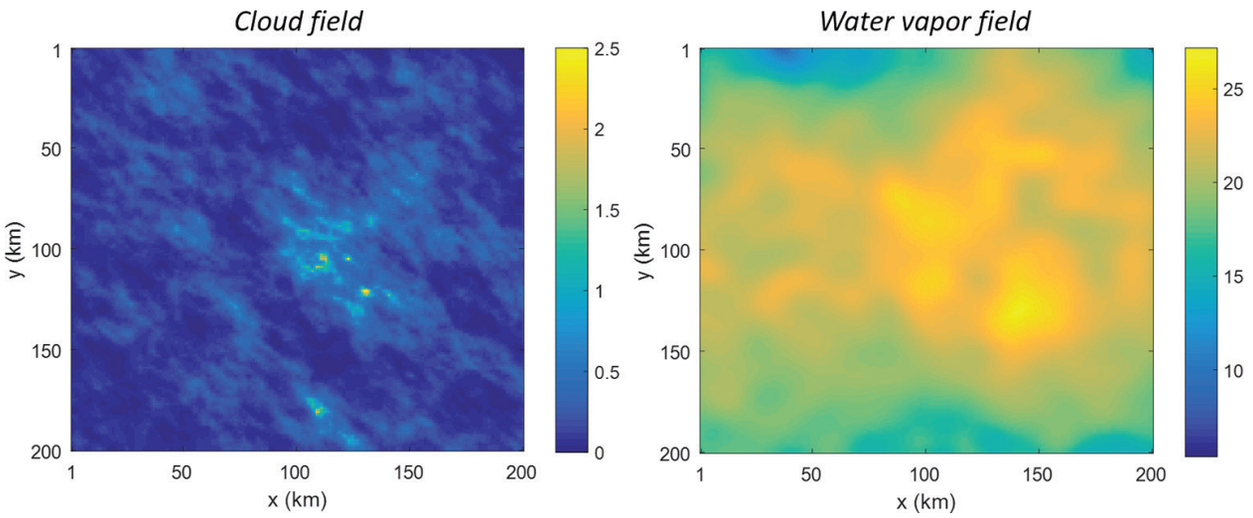

Figure 11. A sample water vapour field generated by SMOV associated to a cloud field synthesized by SMOC.

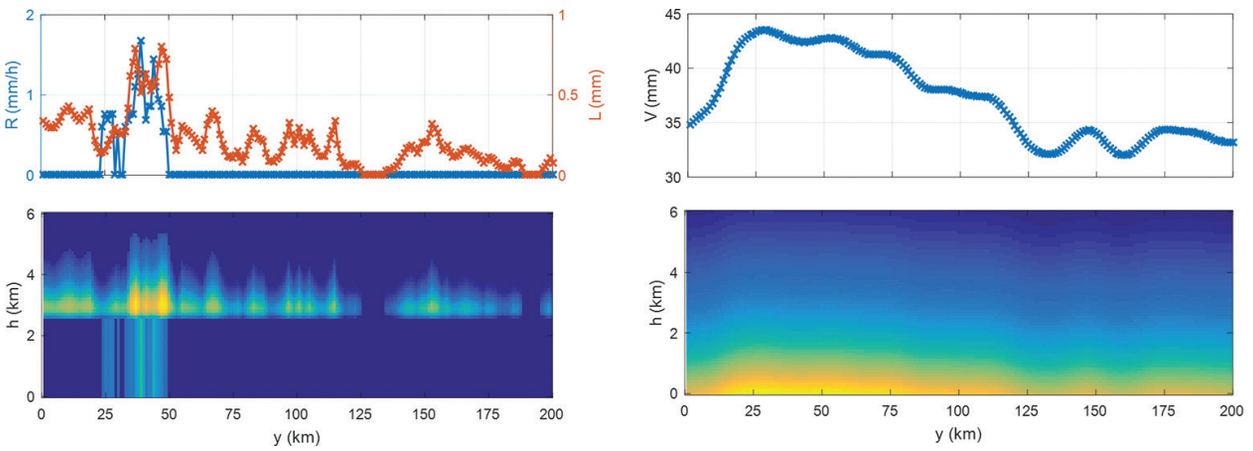

Figure 12. Trend of the rain rate *R*, the integrated liquid water *L* and integrated water vapour *V* along a horizontal line crossing the fields, for a sample of coupled rain rate, cloud and water vapour fields (top part), together with the vertical development of precipitation, clouds and water vapour content (bottom part).

which can indeed be applied to estimate the interaction between electromagnetic waves and the atmosphere in diversified scenarios, including those involving complex system distributed in space, taking advantage of the site diversity concept.

As an example, let us consider a user link operating at 19.7 GHz [16], whose ground station lies close to Milan (latitude 45.4°N, longitude 9.5°E, altitude 84 m a.m.s.l.) and consists of two stations separated by *D* kilometres. The system points to a GEO satellite with orbital positon at 9°E (as the Ka-SAT by Eutelsat) with an elevation angle of 37.8°.

Figure 13 shows the statistics of total attenuation (i.e. including the effects induced by rain, clouds, water vapour and oxygen) estimated by simulating the interaction between the whole set of synthetic maps generated by the physically based models mentioned above and the

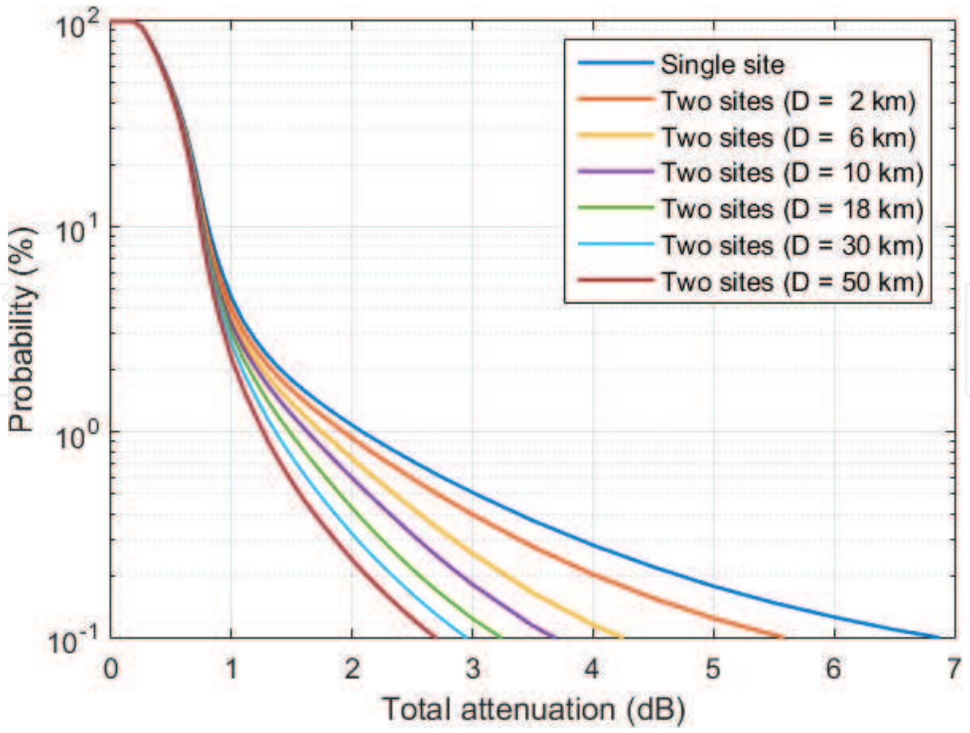

Figure 13. Statistics of total attenuation: two-site diversity system, for different values of separation distance *D*.

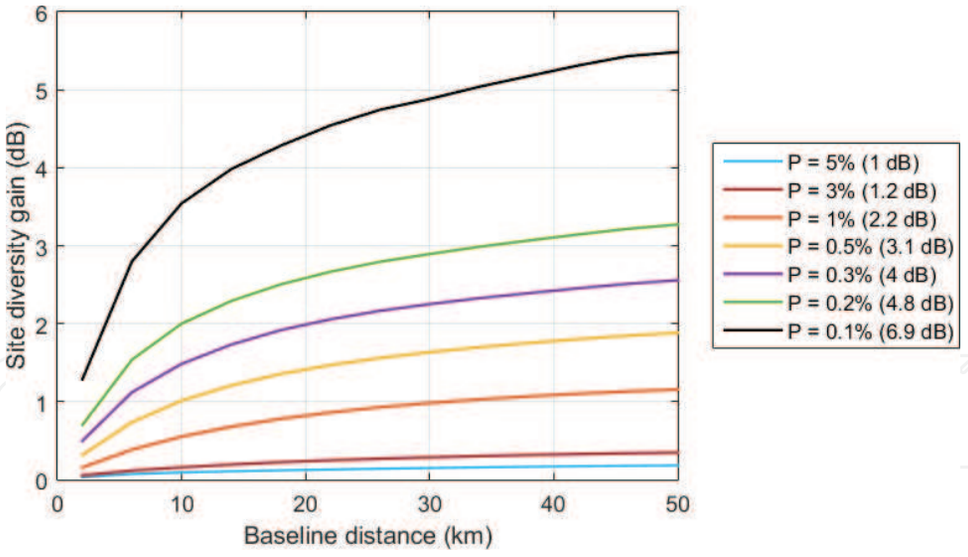

Figure 14. Trend of the site diversity gain *G* as a function of the separation distance *D* and for different outage probabilities of the single-link scenario *P*.

two-site system, for different values of separation distance *D*. The assumption underpinning these results is that the lowest attenuation affecting the two stations is always selected on instantaneous basis (perfect switching). The comparison with the reference single-link case (no site diversity) allows to point out the advantage originating from using two stations: as an

example, the margin needed to cope with the attenuation exceeded for 0.1% of the yearly time varies from approximately 7 to 2.7 dB when employing two stations at 50 km of distance. This is even clearer in **Figure 14**, which depicts the trend of the site diversity gain G as a function of D and for different outage probabilities of the single-link scenario P. G is defined as

$$G(D, P) = A_S(P) - A_J(D, P) \tag{6}$$

where A_S and A_J are the attenuation values of the CCDFs (both for the same probability P), respectively, relative to the single site and to the two-site diversity scheme. As expected, G increases as P decreases (higher probability of intense rainy events) and as the stations are more and more apart (lower degree of correlation). As it turns out, for 99.9% of the time and for distances larger than 30 km, the margin needed to counteract the atmospheric attenuation is lower than roughly 70% of the one required in the single-link scenario. On the other hand, assigning the single-link power margin to the system, the use of two stations leads to a significant increase in the overall data rate, as a higher signal-to-noise ratio allows the use of much more efficient MODCODs [16].

Author details

Lorenzo Luini[1, 2]*, Roberto Nebuloni[2] and Carlo Riva[1, 2]

*Address all correspondence to: lorenzo.luini@polimi.it

1 Department of Electronics, Information and Bioengineering, Politecnico di Milano, Milano, Italy

2 Institute of Electronics, Computer and Telecommunication Engineering, National Research Council of Italy, Milano, Italy

References

[1] P. Mikkonen. Modern 60 GHz radio link. In: Microwave Conference, 1999; Oct. 1999; Munich, Germany. IEEE; 1999. pp. 83–86. DOI: 10.1109/EUMA.1999.338533

[2] M. Grabner, V. Kvicera, G. Timms. 60 GHz Band propagation experiments on terrestrial paths in Sydney and Praha. Radioengineering. 2005;**14**(4):27–32.

[3] M. Ueba, A. Miura, S. Kitazawa, S. Saito, T. Ohira. Feasibility study on millimetre wave multi-gigabit wireless LAN system. In: 2007 European Microwave Conference; Oct. 2007; Munich, Germany. 2007. pp. 688–691. DOI: 10.1109/EUMC.2007.4405285

[4] C. Riva, C. Capsoni, L. Luini, M. Luccini, R. Nebuloni, A. Martellucci. The challenge of using the W band in satellite communication. International Journal of Satellite Communications and Networking. 2013;**32**(3):187–200. DOI: 10.1002/sat.1050

[5] International Telecommunication Union–Radiocommunication Sector. Recommendation ITU-R P.676-10, Attenuation by atmospheric gases [Internet]. 09/2013. Available from: https://www.itu.int/dms_pubrec/itu-r/rec/p/R-REC-P.676-10-201309-I!!PDF-E.pdf [Accessed: May 2016]

[6] International Telecommunication Union – Radiocommunication Sector. Recommendation ITU-R P.836-5, Water vapour: surface density and total columnar content [Internet]. 09/2013. Available from: http://www.itu.int/dms_pubrec/itu-r/rec/p/R-REC-P.836-5-201309-I!!PDF-E.pdf [Accessed: May 2016]

[7] International Telecommunication Union–Radiocommunication Sector. Recommendation ITU-R P.840-6, Attenuation due to clouds and fog [Internet]. 09/2013. Available from: http://www.itu.int/dms_pubrec/itu-r/rec/p/R-REC-P.840-6-201309-I!!PDF-E.pdf [Accessed: May 2016]

[8] International Telecommunication Union–Radiocommunication Sector. Recommendation ITU-R P.838-3, Specific attenuation model for rain for use in prediction methods [Internet]. 03/2005. Available from: http://www.itu.int/rec/R-REC-P.838/en [Accessed: May 2016]

[9] International Telecommunication Union – Radiocommunication Sector. Recommendation ITU-R P.837-6, Characteristics of precipitation for propagation modelling [Internet]. 02/2012. Available from: http://www.itu.int/dms_pubrec/itu-r/rec/p/R-REC-P.837-6-201202-I!!PDF-E.pdf [Accessed: May 2016]

[10] C. Capsoni, M. D'Amico, L. Luini, E. Matricciani, A. Paraboni, C. Riva (Editor), L. Castanet, T. Deloues, V. Fabbro, L. Feral, F. Lacoste, J. Lemorton, E. Kubista, T. Prechtl, M. Schönhuber, "Characterisation and Modelling of Propagation Effects in 20-50 GHz Band", Final report for the European Space Agency under ESTEC Contract No. 17760/03/NL/JA, 2006.

[11] C. Capsoni, L. Luini, A. Paraboni, C. Riva, A. Martellucci. A new prediction model of rain attenuation that separately accounts. IEEE Transactions on Antennas and Propagation. 2009;**57**(1):196–204. DOI: 10.1109/TAP.2008.2009698

[12] L. Luini, C. Capsoni. The SC EXCELL model for the prediction of rain attenuation on terrestrial radio links. Electronics Letters. 2013;**49**(4):307–308. DOI: 10.1049/el.2012.3835

[13] A. Paraboni, A. Martellucci, C. Capsoni, C. Riva. The physical basis of atmospheric depolarization in slant paths in the V band: theory, Italsat experiment and models. IEEE Transactions on Antennas Propagation. 2011;**59**(11):4301–4314. DOI: 10.1109/TAP.2011.2164207

[14] M.M.J.L. Van de Kamp, C. Riva, J.K. Tervonen, E.T. Salonen. Frequency dependence of amplitude scintillation. IEEE Transactions on Antennas and Propagation. 1999;**47**(1):77–85.

[15] B. Evans, P. Thompson, L. Castanet, M. Bousquet and T. Mathiopoulos. Concepts and Technologies for a Terabit/s Satellite. In: SPACOMM; April 2011; Budapest (Hungary).

[16] B. Evans and P. Thompson. Key issues and technologies for a Terabit/s satellite. In: 28th AIAA International Communications Satellite Systems Conference (ICSSC-2010); 30 Aug–2 Sep 2010; Anaheim (California).

[17] P. Angeletti, R. De Gaudenzi, and E. Re. Smart gateways concepts for high-capacity multi-beam networks. In: Proceedings of the 18th Ka and Broadband Communications, Navigation and Earth Observation Conference; 2012; Ottawa (Canada).

[18] R. Nebuloni, C. Capsoni and M. Luccini. Advanced time series synthesizer for simulation of joint rain attenuation conditions. Radio Science. 2014;**49**(9):699–708.

[19] L. Luini, C. Capsoni. A rain cell model for the simulation and performance evaluation of site diversity schemes. IEEE Antennas and Wireless Propagation Letters. 2013; **12**(1):1327–1330.

[20] L. Luini, C. Capsoni. MultiEXCELL: a new rain field model for propagation applications. IEEE Transactions on Antennas and Propagation. 2011;**59**(11):4286–4300.

[21] L. Luini, C. Capsoni. Modeling high resolution 3-D cloud fields for earth-space communication systems. IEEE Transactions on Antennas and Propagation. 2014;**62**(10):5190–5199.

[22] L. Luini, "Modeling and Synthesis of 3-D Water Vapor Fields for EM Wave Propagation Applications", IEEE Transactions on Antennas and Propagation, vol. 64, no. 9, Page(s): 3972 –3980, September 2016.

[23] L. Luini, C. Capsoni. Joint effects of clouds and rain on Ka-band earth observation data downlink systems. European Conference on Antennas and Propagation (EuCAP) 2015, pp. 1–5, 12–17 April 2015; Lisbon, Portugal.

[24] International Telecommunication Union - Radiocommunication Sector. Recommendation ITU-R P.618-12, Propagation data and prediction methods required for the design of earth-space telecommunication systems [Internet]. 07/2015. Available from: https://www.itu.int/rec/R-REC-P.618-12-201507-I/en [Accessed: May 2016]

IntechOpen